IX CONGRESSO BRASILEIRO DE
ENGENHARIA E CIÊNCIAS TÉRMICAS
9th BRAZILIAN CONGRESS OF THERMAL
ENGINEERING AND SCIENCES

Paper CIT02-0392

MISALIGNMENT EFFECTS ON THE BEHAVIOR OF SPIRAL GROOVE GAS FACE SEALS

Marco Túlio C. Faria
Universidade Federal de Minas Gerais
Departamento de Engenharia Mecânica
Av. Antônio Carlos, 6627
Belo Horizonte – MG – 31270-901 - Brasil
mtfaria@dedalus.lcc.ufmg.br

Abstract. *This paper deals with a finite element analysis of spiral groove gas face seals operating at high speeds. A high-order finite element procedure, based on the Galerkin weighted residual method, is implemented to predict some static and dynamic performance characteristics of grooved gas face seals. Seal opening force, flow rate and dynamic force coefficients are computed with respect to the seal face static misalignment. Curves of seal characteristics depict the influence of the seal face misalignment on the behavior of grooved gas face seals.*

Keywords*. Face Seals, Noncontacting Seals, Grooved Seals, Gas Seals, Finite Element*

1. Introduction

Modern environmental laws have required the development of very efficient sealing systems capable of preventing release of harmful fluids from industrial turbomachinery into atmosphere. Seal manufacturers have worked on zero fluid emission face seal designs for clean environment (Burgmann, 1997). Increasing productivity in the process industry demands the development of high speed mechanical face seals, which are subjected to stringent operating conditions. Hence the analysis and design of sealing systems require the development of accurate numerical procedures able to predict the performance characteristics of high speed gas face seals.

In order to increase the seal opening force and decrease fluid leakage, grooves have been introduced into the noncontacting seal faces. Successful sealing systems have employed spiral groove gas face seals (SGGFS) (Klostermann, 1999; Wu et all, 1999). Even though grooved gas seals have encountered many applications in the chemical, petrochemical, pulp and paper and food processing industries, predictions and experimental measurements of SGGFS static and dynamic performance characteristics have not been reported in the technical literature.

Some recent computational procedures based on the finite element method (FEM) have been implemented to analyze the behavior of grooved gas face seals. Bonneau et all (1993) implement an efficient finite element procedure based on the Petrov-Galerkin residual method to determine the opening forces and leakage flow rates of aligned SGGFSs operating at low and medium speeds. Tournerie et all (1994) employ the Bonneau et all´s procedure to predict some steady-steate performance characteristics of misaligned SGGFSs operating at low speeds. Finally, a finite element analysis, based on the Galerkin weighted residual method, of low speed aligned SGGFSs is carried out by Hernandez and Boudet (1995) to predict some of their steady-state performance characteristics.

This paper presents a finite element formulation specially devised to analyze the spiral groove gas face seal behavior at high speeds. Static face misalignment is included into the finite element formulation. An efficient finite element procedure (Faria, 2001), based on a high-order Galerkin method, is implemented to solve the Reynolds equation for compressible fluids. A linearized perturbation procedure is used on the classical Reynolds equation in order to render the zero-th and first order lubrication equations, which allow, respectively, the prediction of the opening force and the dynamic force coefficients for misaligned noncontacting gas face seals. The finite element analysis shows the influence of the static face misalignment on some seal steady-state and dynamic performance characteristics.

2. Description of the Problem

Figure (1) presents the geometry and parameters describing a gas-lubricated spiral groove face seal (SGGFS). The seal configurations are described following the same procedure as that used by Zirkelback and San Andrés (1999). The seal geometry includes the ridge clearance c, the grove depth c_g, the ridge width w_r, the groove width w_g, the number of grooves N_g, the groove angle β, the seal inner radius r_i, the seal outer radius r_o, the seal grooved portion inner radius r_{gi} and the seal grooved portion outer radius r_{go}. The groove depth ratio $\delta = c_g / c$, the groove width ratio $\alpha_g = w_g / (w_r + w_g)$ and the seal dam extent $l = (r_{gi} - r_i) / (r_o - r_i)$ are dimensionless geometric parameters widely used in the description of the seal geometry. The seal configuration is described in relation to a coordinate system attached to

the grooved seal face. The (r,θ, z) coordinate system is attached to the rotating grooves at speed Ω. The (r,Φ, z) coordinate system is attached to the stationary face. The relation between the two coordinate systems is given by Φ=θ+Ωt. The equation governing the logarithmic spiral contour of the grooves is $r = r_{gi} e^{\theta \tan(\beta)}$ (Muijderman, 1966).

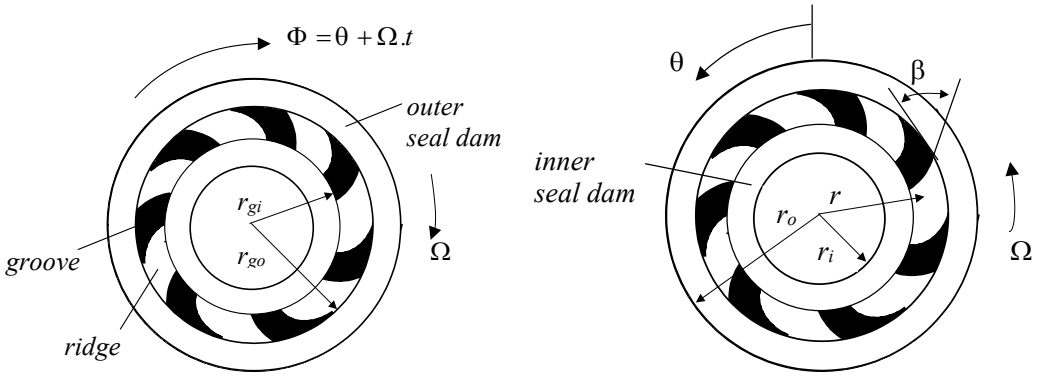

(a) Stationary Grooved Face

(b) Rotating Grooved Face

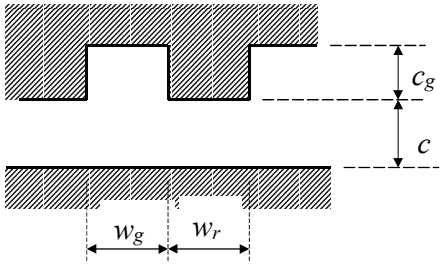

$$\delta = c_g / c$$

$$\alpha_g = w_g / (w_r + w_g)$$

(c) Detail of a ridge-groove pair

Figure 1. Geometry and parameters of a SGGFS with rotating and stationary grooved surface.

Grooves are etched either on the rotating surface or on the stationary surface of the seal. The relative motion between the grooved and smooth surfaces causes a pumping action in the fluid. Pumping-in (inwardly pumping) and pumping-out (outwardly pumping) seal designs usually find applications in industrial rotating machinery (Muijderman, 1966). Sealing pressure dams are generally employed in SGGFS configurations either to minimize leakage or increase axial stiffness. Inner and outer pressure dams are introduced into the grooved surface to enhance the seal performance.

The laminar flow of an isothermal, isoviscous ideal gas within the film lands of a spirally grooved face seal (Faria, 2001) is described by

$$\frac{1}{r}\frac{\partial}{\partial\theta}\left(\frac{ph^3}{12\mu}\frac{1}{r}\frac{\partial p}{\partial\theta}\right)+\frac{1}{r}\frac{\partial}{\partial r}\left(\frac{ph^3}{12\mu}r\frac{\partial p}{\partial r}\right)=\frac{B\Omega}{2r}\frac{\partial}{\partial\theta}(rph)+\frac{\partial(ph)}{\partial t} \tag{1}$$

Here, p represents the hydrodynamic pressure, h is the fluid film thickness, and μ is the fluid viscosity. B is a seal parameter that describes the groove rotation direction. Table (1) shows the values of B for the different seal configurations (Faria, 2001).

Table 1. The groove rotation direction parameter with seal configuration.

Groove Angle (β) Range	Stationary Grooves	Rotating Grooves
$0^o < \beta < 90^o$	Outward Pumping (B = -1)	Inward Pumping (B = 1)
$90^o < \beta < 180^o$	Inward Pumping (B = 1)	Outward Pumping (B = -1)

The seal is subjected to pressures p_{in} and p_{out} at its inner and outer radii r_i and r_o, respectively. Typically $p_{out} > p_{in}$. In a seal, the inner and outer radii sections are open allowing radial flow inward and outward. The pressure distribution is periodic over the seal/bearing circumferential length.

The fluid film thickness is described accounting for the static misalignments of the seal surface (Jang and Kim, 1999). The seal moving surface has three degrees of freedom, schematically shown in Fig. (2). The film thickness h_o at an equilibrium position can be written as

$$h_o(r,\theta) = c + r\varphi_{y_o}\cos\theta - r\varphi_{x_o}\sin\theta\ , \qquad \text{in the ridge region} \tag{2}$$

$$h_o(r,\theta) = c + c_g + r\varphi_{y_o}\cos\theta - r\varphi_{x_o}\sin\theta\ , \qquad \text{in the groove region.} \tag{3}$$

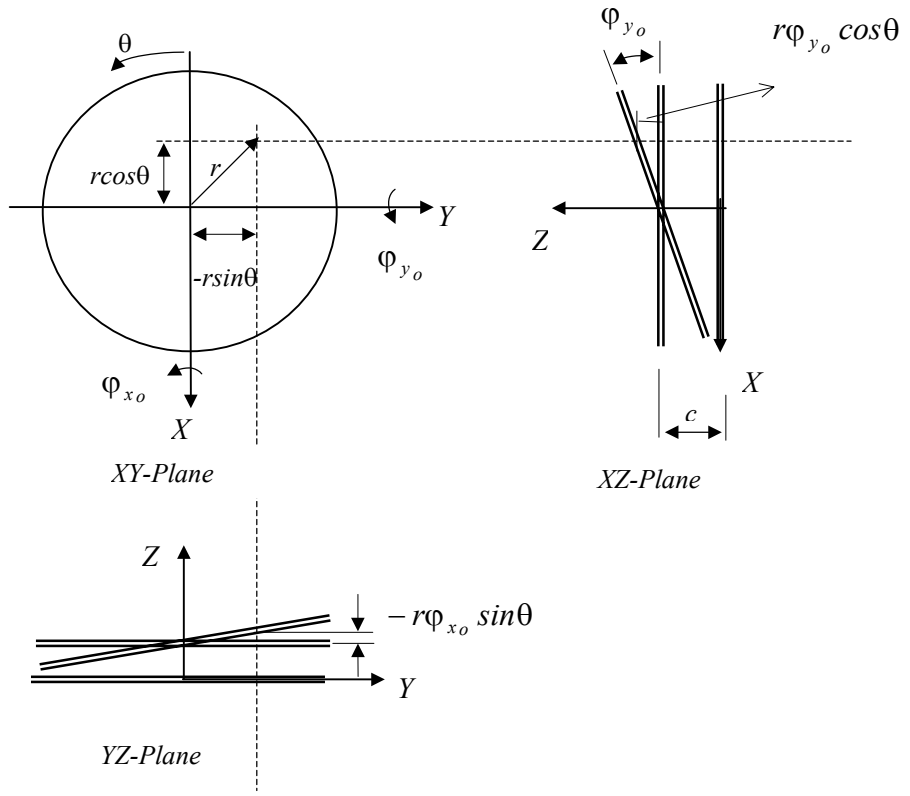

Figure 2. Equilibrium position of a misaligned moving surface.

φ_{x_o} and φ_{y_o} describe the angular position of the moving surface at equilibrium, i.e. are small angular displacements representing the face misalignment about axes *X* and *Y*, respectively.

3. Lubrication Equations

A linearized perturbation procedure (Lund, 1987) is performed on the Reynolds equation (Eq. (1)) to render the zeroth- and first-order lubrication equations. Small dynamic perturbations ΔZ, $\Delta\varphi_x$, and $\Delta\varphi_y$ at excitation frequency ω about an equilibrium position of the moving rotating face cause perturbations in the film thickness and pressure distributions. The perturbed film thickness *h(r,θ,t)* is given by

$$h(r,\theta,t) = h_o(r,\theta) + r\cos\theta.\Delta\varphi_y e^{i\omega t} - r\sin\theta.\Delta\varphi_x e^{i\omega t} + \Delta Z.e^{i\omega t} \tag{4}$$

where $i = \sqrt{-1}$. The perturbed pressure field is expressed as

$$p(r,\theta,t) = p_o(r,\theta) + p_z(r,\theta)\Delta Z e^{i\omega t} + p_{\varphi_x}(r,\theta)\Delta\varphi_x e^{i\omega t} + p_{\varphi_y}(r,\theta)\Delta\varphi_y e^{i\omega t} \tag{5}$$

where p_o represents the zeroth-order pressure field, and p_z, p_{φ_x}, and p_{φ_y} are the first-order pressure distributions caused by the small perturbations. Expressions for the linearized zeroth- and first-order lubrication equations are obtained by substituting Eq. (4) and Eq. (5) into Eq. (1). The zeroth-order lubrication equation has the following form.

$$\frac{1}{r}\frac{\partial}{\partial\theta}\left(\frac{p_o h_o^3}{12\mu}\frac{1}{r}\frac{\partial p_o}{\partial\theta} - \frac{B\Omega r}{2}p_o h_o\right) + \frac{1}{r}\frac{\partial}{\partial r}\left(\frac{p_o h_o^3}{12\mu}r\frac{\partial p_o}{\partial r}\right) = 0 \tag{6}$$

The first-order equation for axial displacement Z is expressed as

$$\frac{1}{r}\frac{\partial}{\partial\theta}\left(\frac{3h_o^2}{12\mu r}p_o\frac{\partial p_o}{\partial\theta}+\frac{h_o^3}{12\mu r}\frac{\partial(p_o p_z)}{\partial\theta}-\frac{B\Omega r}{2}\left(p_z h_o+p_o\right)\right)+ \frac{1}{r}\frac{\partial}{\partial r}\left[r\left(\frac{3h_o^2}{12\mu}p_o\frac{\partial p_o}{\partial r}+\frac{h_o^3}{12\mu}\frac{\partial(p_o p_z)}{\partial r}\right)\right]=i\omega(p_z h_o+p_o) \tag{7}$$

The first-order equations for the dynamic angular displacements φ_x and φ_y around the X and Y axes are given by

$$\frac{1}{r}\frac{\partial}{\partial\theta}\left(\frac{-3h_o^2 r\sin\theta}{12\mu r}p_o\frac{\partial p_o}{\partial\theta}+\frac{h_o^3}{12\mu r}\frac{\partial(p_o p_{\varphi x})}{\partial\theta}-\frac{B\Omega r}{2}\left(p_{\varphi x}h_o-p_o r\sin\theta\right)\right)+ \frac{1}{r}\frac{\partial}{\partial r}\left[r\left(\frac{-3h_o^2 r\sin\theta}{12\mu}p_o\frac{\partial p_o}{\partial r}+\frac{h_o^3}{12\mu}\frac{\partial(p_o p_{\varphi x})}{\partial r}\right)\right]=i\omega(p_{\varphi x}h_o-p_o r\sin\theta) \tag{8}$$

$$\frac{1}{r}\frac{\partial}{\partial\theta}\left(\frac{3h_o^2 r\cos\theta}{12\mu r}p_o\frac{\partial p_o}{\partial\theta}+\frac{h_o^3}{12\mu r}\frac{\partial(p_o p_{\varphi y})}{\partial\theta}-\frac{B\Omega r}{2}\left(p_{\varphi y}h_o+p_o r\cos\theta\right)\right)+ \frac{1}{r}\frac{\partial}{\partial r}\left[r\left(\frac{3h_o^2 r\cos\theta}{12\mu}p_o\frac{\partial p_o}{\partial r}+\frac{h_o^3}{12\mu}\frac{\partial(p_o p_{\varphi y})}{\partial r}\right)\right]=i\omega(p_{\varphi y}h_o+p_o r\cos\theta) \tag{9}$$

4. Finite Element Procedure for the Lubrication Equations

An efficient finite element procedure is implemented for the solution of the perturbed lubrication equations. The solution procedure is based on the Galerkin weighted residual method and uses high-order shape functions $\left\{\psi_j^e\right\}_{j=1,2,3,4}$, which are derived from an approximate solution to the non-linear Reynolds equation within an element (Faria, 2001). The fluid flow domain within the seal lands is divided into four-node isoparametric finite elements Ω_e with boundary given by Γ_e. The zeroth-order pressure field is interpolated over the element domain in the following form.

$$p_o^e=\sum_{i=1}^{4}\psi_i^e p_{oi}^e \tag{10}$$

where p_{oi}^e are the nodal values of pressure on the element *(e)*. By employing the Galerkin weighted residual method and substituting Eq. (10) into Eq. (6) render the following zeroth-order finite element system of asymmetric equations

$$K_{ji}^e.p_{oi}^e=q_j^e \quad ,i,j=1,2,3,4 \tag{11}$$

where

$$K_{ji}^e=\iint_{\Omega_e}\left\{\frac{p_o h_o^3}{12\mu}\left(\frac{\partial\psi_i^e}{\partial r}\frac{\partial\psi_j^e}{\partial r}+\frac{1}{r^2}\frac{\partial\psi_i^e}{\partial\theta}\frac{\partial\psi_j^e}{\partial\theta}\right)-\frac{B\Omega h_o}{2}\psi_i^e\frac{\partial\psi_j^e}{\partial\theta}\right\}d\Omega_e \tag{12}$$

$$q_j^e=-\oint_{\Gamma_e}\psi_j^e\dot{m}_n d\Gamma_e \tag{13}$$

$\dot{m}_n$ is the zeroth-order mass flow rate normal to the element boundary. A successive substitution procedure is implemented to solve iteratively the system of zeroth-order finite element equations (Faria, 2001).

The finite element equations for the first-order pressures are obtained in a similar way. The pressures p_z, $p_{\varphi x}$, and $p_{\varphi y}$ are interpolated within an element domain in the following form.

$$p_z^e = \sum_{i=1}^{4} \psi_i^e \, p_{z\,i}^e \tag{14}$$

$$p_{\varphi\,x}^e = \sum_{i=1}^{4} \psi_i^e \, p_{\varphi\,x\,i}^e \tag{15}$$

$$p_{\varphi\,y}^e = \sum_{i=1}^{4} \psi_i^e \, p_{\varphi\,y_i}^e \tag{16}$$

Then the finite element first-order equation for axial displacements Z is expressed as

$$K_{z\,ji}^e . p_{z\,i}^e = q_{z\,j}^e + f_{z\,j}^e \qquad , \; i,j=1,2,3,4 \tag{17}$$

where

$$K_{z\,ji}^e = \iint_{\Omega_e} \left[\frac{p_o^e h_o^3}{12\mu} \left(\frac{\partial \psi_j^e}{\partial r} \frac{\partial \psi_i^e}{\partial r} + \frac{1}{r^2} \frac{\partial \psi_j^e}{\partial \theta} \frac{\partial \psi_i^e}{\partial \theta} \right) + \frac{h_o^3}{12\mu} \left(\frac{\partial \psi_j^e}{\partial r} \frac{\partial p_o^e}{\partial r} + \frac{1}{r^2} \frac{\partial \psi_j^e}{\partial \theta} \frac{\partial p_o^e}{\partial \theta} \right) \psi_i^e - \frac{B\Omega h_o}{2} \frac{\partial \psi_j^e}{\partial \theta} \psi_i^e + i\omega h_o \psi_j^e \psi_i^e \right] d\Omega_e \tag{18}$$

$$q_{z\,j}^e = - \oint_{\Gamma_e} \psi_j^e \dot{m}_{z\,n} \, d\Gamma_e \tag{19}$$

$$f_{z\,j}^e = \iint_{\Omega_e} \left(\frac{-3h_o^2}{12\mu} p_o^e \left(\frac{\partial \psi_j^e}{\partial r} \frac{\partial p_o^e}{\partial r} + \frac{1}{r^2} \frac{\partial \psi_j^e}{\partial \theta} \frac{\partial p_o^e}{\partial \theta} \right) + \frac{B\Omega p_o^e}{2} \frac{\partial \psi_j^e}{\partial \theta} - i\omega p_o^e \psi_j^e \right) d\Omega_e . \tag{20}$$

The first-order mass flow rate outward the element boundary is given by $\dot{m}_{z\,n}$.

The finite element systems of equations for the first-order equations for angular displacements φ_x and φ_y are given by

$$K_{\varphi\,x\,ji}^e . p_{\varphi\,x\,i}^e = q_{\varphi\,x\,j}^e + f_{\varphi\,x\,j}^e \; , \; i,j=1,2,3,4 \tag{21}$$

$$K_{\varphi\,y\,ji}^e . p_{\varphi\,y_i}^e = q_{\varphi\,y\,j}^e + f_{\varphi\,y\,j}^e \; , \; i,j=1,2,3,4 \tag{22}$$

where

$$K_{\varphi\,x\,ji}^e = K_{z\,ji}^e \tag{23}$$

$$K_{\varphi\,y\,ji}^e = K_{z\,ji}^e \tag{24}$$

$$q_{\varphi\,x\,j}^{\;e} = - \oint_{\Gamma_e} \psi_j^e \dot{m}_{x\,n} \, d\Gamma_e \tag{25}$$

$$q_{\varphi\,y\,j}^{\;e} = - \oint_{\Gamma_e} \psi_j^e \dot{m}_{y\,n} \, d\Gamma_e \tag{26}$$

$$f_{\varphi\,x\,j}^e = \iint_{\Omega_e} \left\{ \frac{3h_o^2 r \sin\theta}{12\mu} p_o^e \left(\frac{\partial \psi_j^e}{\partial r} \frac{\partial p_o^e}{\partial r} + \frac{1}{r^2} \frac{\partial \psi_j^e}{\partial \theta} \frac{\partial p_o^e}{\partial \theta} \right) - \frac{B\Omega r \sin\theta}{2} p_o^e \frac{\partial \psi_j^e}{\partial \theta} + i\omega p_o^e r \sin\theta \psi_j^e \right\} d\Omega_e \tag{27}$$

$$f_{\varphi\,y\,j}^e = \iint_{\Omega_e} \left\{ \frac{-3h_o^2 r \cos\theta}{12\mu} p_o^e \left(\frac{\partial \psi_j^e}{\partial r} \frac{\partial p_o^e}{\partial r} + \frac{1}{r^2} \frac{\partial \psi_j^e}{\partial \theta} \frac{\partial p_o^e}{\partial \theta} \right) + \frac{B\Omega r \cos\theta}{2} p_o^e \frac{\partial \psi_j^e}{\partial \theta} - i\omega p_o^e r \cos\theta \psi_j^e \right\} d\Omega_e \tag{28}$$

where $\dot{m}_{x_n}$ and $\dot{m}_{y_n}$ are the first-order mass flow rates outward Γ_e.

5. Steady-State and Dynamic Performance Characteristics

The finite element equations (11), (17), (21) e (22) are assembled for the whole seal domain. The zeroth- and first-order pressure fields are computed by solving the global finite element equations (Faria, 2001). Seal opening force (F_z) and restoring moments ($M_{\varphi x}, M_{\varphi y}$) are given by the following expression.

$$\begin{Bmatrix} F_z \\ M_{\varphi x} \\ M_{\varphi y} \end{Bmatrix} = \iint_{\Omega} \begin{Bmatrix} (p_o - p_{ref}) \\ -(p_o - p_{ref}) r \sin\theta \\ (p_o - p_{ref}) r \cos\theta \end{Bmatrix} r d\theta dr \tag{29}$$

where p_{ref} represents the reference pressure defined as the lowest pressure of the seal inner and outer pressures. The dynamic force and moment coefficients are given by

$$K_{\sigma\beta} + i\omega C_{\sigma\beta} = -\iint_{\Omega} h_\sigma \, p_\beta \, r d\theta dr \qquad , \ \sigma, \beta = Z, \varphi_x, \varphi_y \tag{30}$$

where $h_Z = 1$, $h_{\varphi x} = -r\sin\theta$, and $h_{\varphi y} = r\cos\theta$. Equation (30) is rewritten in matrix form as

$$\begin{bmatrix} K_{zz} & K_{z\varphi_x} & K_{z\varphi_y} \\ K_{\varphi_x z} & K_{\varphi_x\varphi_x} & K_{\varphi_x\varphi_y} \\ K_{\varphi_y z} & K_{\varphi_y\varphi_x} & K_{\varphi_y\varphi_y} \end{bmatrix} + i\omega \begin{bmatrix} C_{zz} & C_{z\varphi_x} & C_{z\varphi_y} \\ C_{\varphi_x z} & C_{\varphi_x\varphi_x} & C_{\varphi_x\varphi_y} \\ C_{\varphi_y z} & C_{\varphi_y\varphi_x} & C_{\varphi_y\varphi_y} \end{bmatrix} = \iint_{\Omega} \begin{Bmatrix} -1 \\ r\sin\theta \\ -r\cos\theta \end{Bmatrix} \begin{Bmatrix} p_z & p_{\varphi x} & p_{\varphi y} \end{Bmatrix} r d\theta dr \ . \tag{31}$$

5. Numerical Predictions

This section is divided into two parts: 5.1.Validation and 5.2.Performance Characteristics of SGGFSs. An example of mechanical gas face seal is selected to evaluate the accuracy of the finite element procedure implemented for SGGFSs. Results computed by this procedure are compared with predictions available in the literature for aligned gas seals. Then, the influence of the static face misalignment on gas grooved face seals is shown through some performance characteristic curves.

5.1. Validation

Predictions obtained by the high-order FEM procedure (Faria, 2001) for axial stiffness and damping coefficients of aligned gas face seals are compared with those obtained by the incremental Galerkin FEM scheme implemented by Zirkelback and San Andrés (1999). The seal parameters are given in Table (2) with c = 6 μm. Figures (3) and (4) present the dimensionless axial stiffness and damping coefficients for a SGGFS versus the frequency number ($\sigma = 2\Lambda(\omega/\Omega)$), respectively, at three speed numbers ($\Lambda = \frac{6\mu\Omega}{p_{ref}}\left(\frac{r_o}{c}\right)^2$), computed by both the incremental FEM (dashed line) and the high-order FEM (solid line) schemes. Both schemes render practically the same results for low speed number problems.

Table 2. SGGFS parameters for validation.

r_i = 0.062 m	(*stationary grooves*)	c = 6 μm
r_{gi} = 0.069 m	Ω = *4774.7 rpm*	c_g = 6 μm
r_o = 0.0805 m	ρ = 1.09 kg/m^3	μ = 18x10^{-6} Pa.s
β =161.4^o		p_i = 0.1 MPa
N_g = 12 grooves		p_o = 0.3 MPa
α_g = 0.567		Λ *varies from 5 to 100*

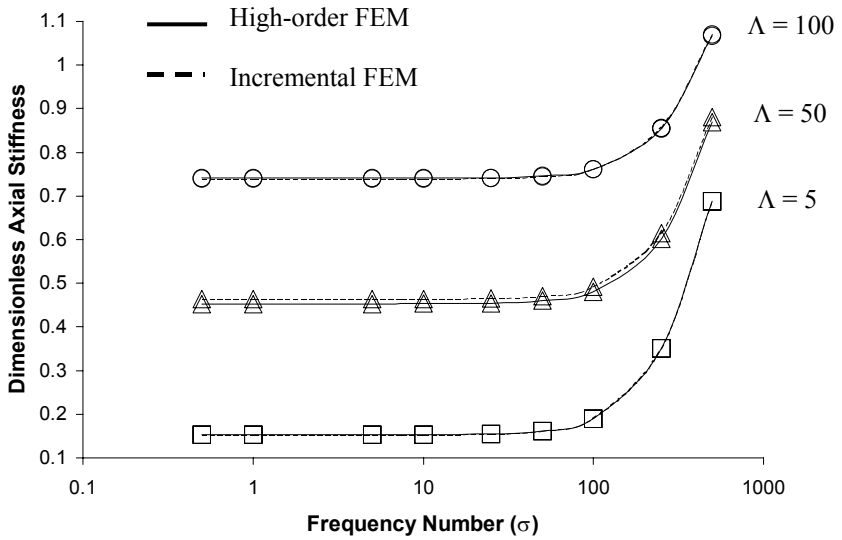

Figure 3. Comparative results for dimensionless axial stiffness versus frequency number in a SGGFS.

400 finite elements are used to model a ridge-groove pair in both procedures. The predictions by the incremental FEM scheme are computed using five steps and step increment of 0.05Λ. The normalization for stiffness and damping coefficients is shown in Tab. (3).

Table 3. Normalization of force coefficients for gas face seal from Tab. (2).

Normalized Stiffness	Normalized Damping
$\overline{K}_{zz} = K_{zz} /(\pi p_{ref}(r_o^2 - r_i^2)/c)$	$\overline{C}_{zz} = C_{zz} /(\pi p_{ref}(r_o^2 - r_i^2)/c\Omega)$

5.2. Performance Characteristics of SGGFSs

The influence of the static misalignment on the performance characteristics of spirally grooved gas face seals is analyzed at moderate and high speed numbers (Λ). The seal baseline geometry for this analysis is given in Tab. (4), and represents a high speed inward pumping gas seal employed in nitrogen pumps.

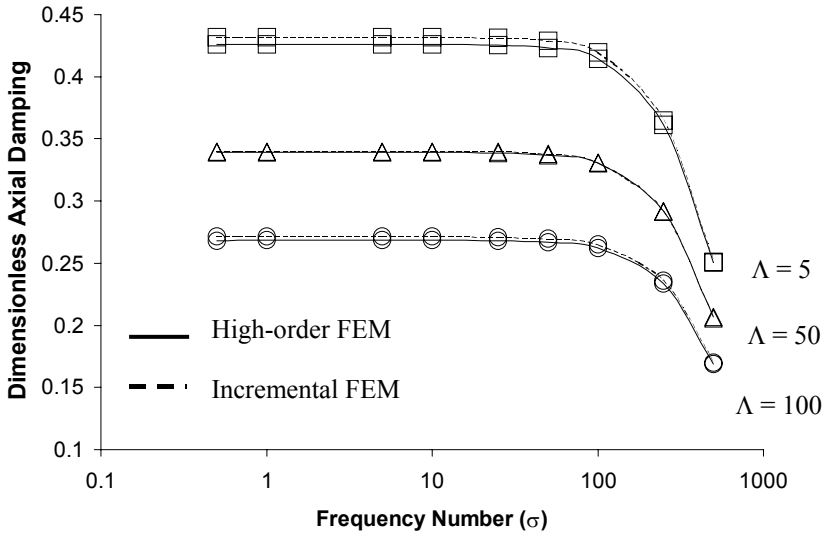

Figure 4. Comparative results for dimensionless axial damping versus frequency number in a SGGFS.

The seal performance characteristics are evaluated with respect to the static misalignment about the axis *X*. In this study, the fixed seal face (stationary face) is slightly misaligned and the flexibly mounted face is perfectly aligned. Coning effects are not taken into account in the computations. The misalignment angle is given in degrees. The minimum and maximum values of seal outer clearances are about 0.9 μm and 4.1 μm (for φ_x=0.001°), respectively.

Table (5) shows the normalization of the seal opening force ($\overline{F}_z$), leakage flow rate ($\overline{Q}$), restoring moments ($\overline{M}_{\varphi_x}, \overline{M}_{\varphi_y}$), and stiffness coefficients ($\overline{K}_{ij}$) employed in this work. R_g represents the gas constant.

Table 4. Geometric and operating parameters for a SGGFS.

	Stationary grooves	
r_i = 0.07112 m	β = 160°	p_{in} =0.101 MPa
r_{gi} = 0.076454 m	α_g = 0.5	p_{out} = 0.505 MPa
r_o = 0.0889 m	N_g =12 *grooves*	Λ = 300 or 1253
$c = c_g$ = 2.54 μm	μ = 10.963x10^{-6} Pa.s	(Ω = 3600 or 15000 rpm)
	Mesh: 1320 elements	
	(132 circumferential x 10 radial elements)	

Table 5. Normalization parameters for seal performance characteristics.

$\overline{F}_z = F_z / F^*$	$F^* = p_{av}\pi(r_o^2 - r_i^2)$	$p_{av} = (p_o + p_i)/2$
$\overline{Q} = Q/Q^*$	$Q^* = \dfrac{\pi\rho_{av}(c+c_g)^3 p^*}{6\mu\, ln(r_o/r_i)}$	$\rho_{av} = \dfrac{p_o + p_i}{2R_g T}$
	where $p^* = (p_i - p_o)$	
$\overline{M}_i = M_i/M^*$; i=φ_x,φ_y	$M^* = F^* r_o$	
Axial stiffness :	$\overline{K}_{zz} = K_{zz}/K^*_{zz}$	$K^*_{zz} = F^*/c$
Angular stiffness:	$\overline{K}_{ij} = K_{ij}/K^*_{xx}$; i,j=φ_x,φ_y	$K^*_{xx} = \dfrac{F^* r_o^2}{c}$
Cross-Coupled Stiffness:	$\overline{K}_{zi} = K_{zi}/K^*_{xz}$; i=φ_x,φ_y	$K^*_{xz} = F^* r_o/c$
	$\overline{K}_{iz} = K_{iz}/K^*_{xz}$	

Figure (5) shows the dimensionless seal opening force ($\overline{F}_z$) and inward flow rate ($\overline{Q}$) versus misalignment about the axis X (φ_x) at moderate (dashed line) and high speed numbers (solid line). $\overline{Q}$ and $\overline{F}_z$ increase with increasing φ_x. The misalignment generates regions of converging and diverging clearances in the circumferential direction. The hydrodynamic pressure increases in the region of converging clearances.

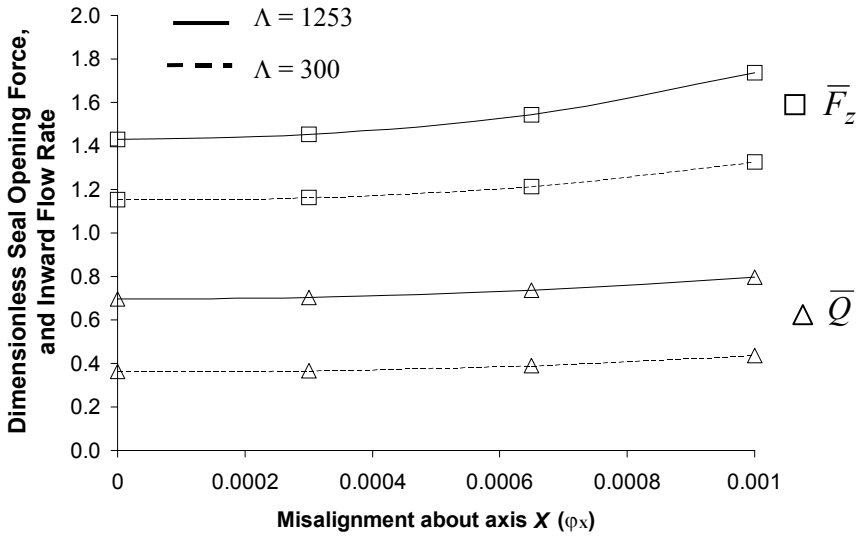

Figure 5. Dimensionless opening force and flow rate versus misalignment angle in a SGGFS.

Figure (6) depicts the restoring moments about axes *X* and *Y* ($\overline{M}_{\varphi_y}$, $\overline{M}_{\varphi_x}$) versus the static misalignment about the axis *X*. Misalignment on axis *X* (φ_x) induces hydrodynamic moment acting transversely to the axis of tilt (Etsion, 1979). $\overline{M}_{\varphi_x}$ is directly in opposition to the tilt angle. $\overline{M}_{\varphi_y}$ is coupled to the angular displacement about the axis *X* due to the wedge effect. The higher is the speed number, the larger is the seal ability to resist angular motions on the axis of tilt.

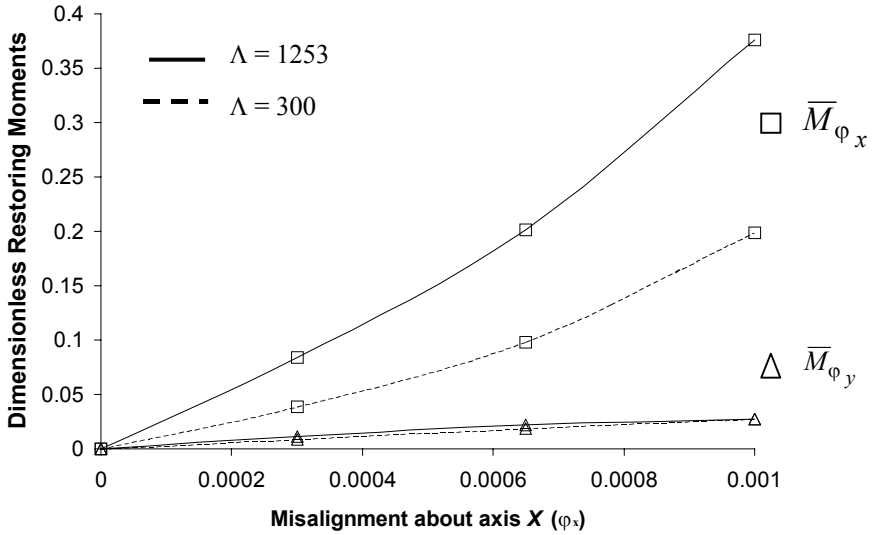

Figure 6. Dimensionless restoring moments versus misalignment angle in a SGGFS.

The static dimensionless stiffness coefficients versus misalignment are shown in Fig. (7), (8) and (9). Figure (7) shows that the direct stiffness coefficients increase as φ_x increases for moderate (dashed line) and high (solid line) speed numbers. Figures (8) and (9) depict the cross-coupled stiffness coefficients at moderate (Λ=300) and high speed (Λ=1253) numbers, respectively. As expected, the cross-coupled coefficients associated with the coupling between the axial and tilt motions ($\overline{K}_{z\varphi_x}$, $\overline{K}_{\varphi_x z}$) vary significantly with increasing misalignment angle about axis *X*.

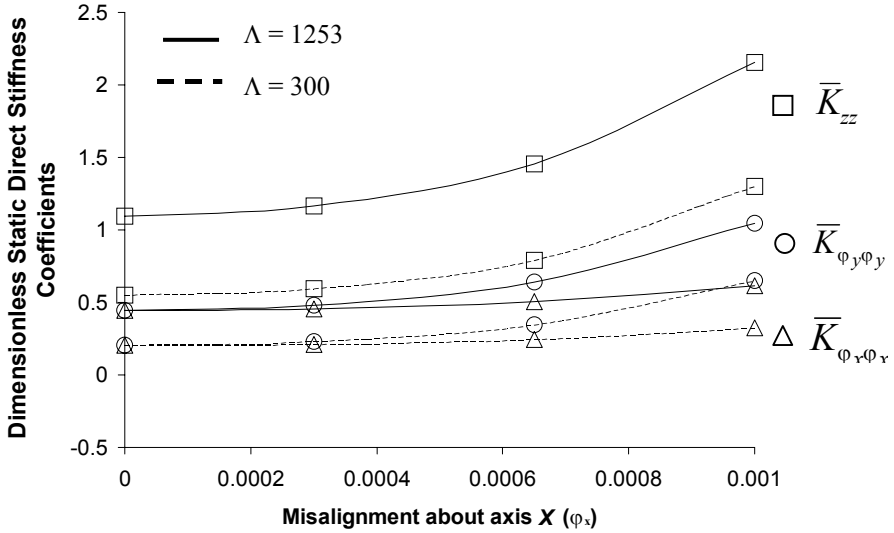

Figure 7. Dimensionless direct static stiffness coefficients versus misalignment angle in a SGGFS.

To illustrate the frequency dependence of force coefficients for misaligned SGGFSs operating at high speed number (Λ=1253), Figure (10) depicts the variation of the dimensionless direct stiffness with respect to frequency number (σ) at two values of misalignment angle (φ_x). Dashed line is associated with frequency-dependent coefficients computed for φ_x=0.0004° and solid line for φ_x=0.0008°. Direct stiffness coefficients practically do not vary with increasing frequency numbers.

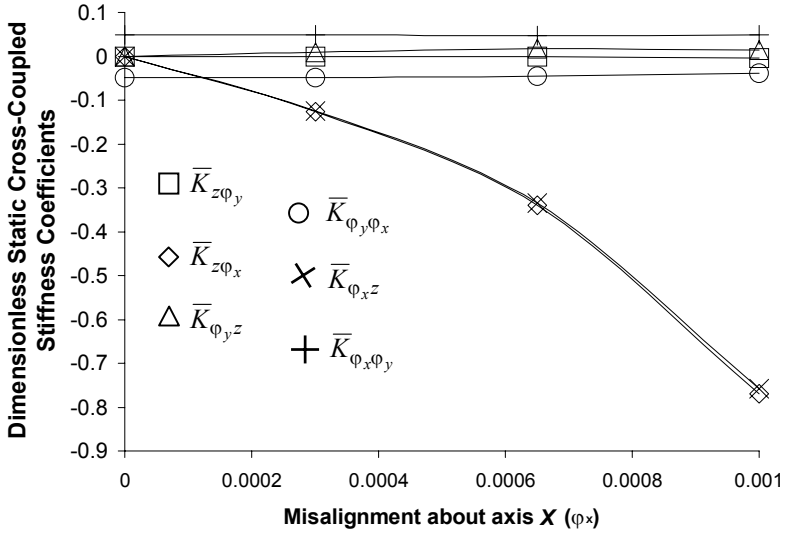

Figure 8. Dimensionless cross-coupled static stiffness coefficients versus misalignment angle in a SGGFS (Λ=300).

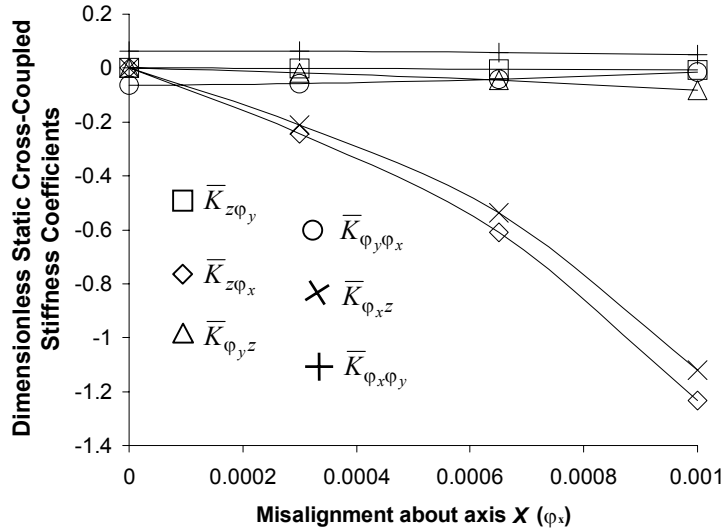

Figure 9. Dimensionless cross-coupled static stiffness coefficients versus misalignment angle in a SGGFS (Λ=1253).

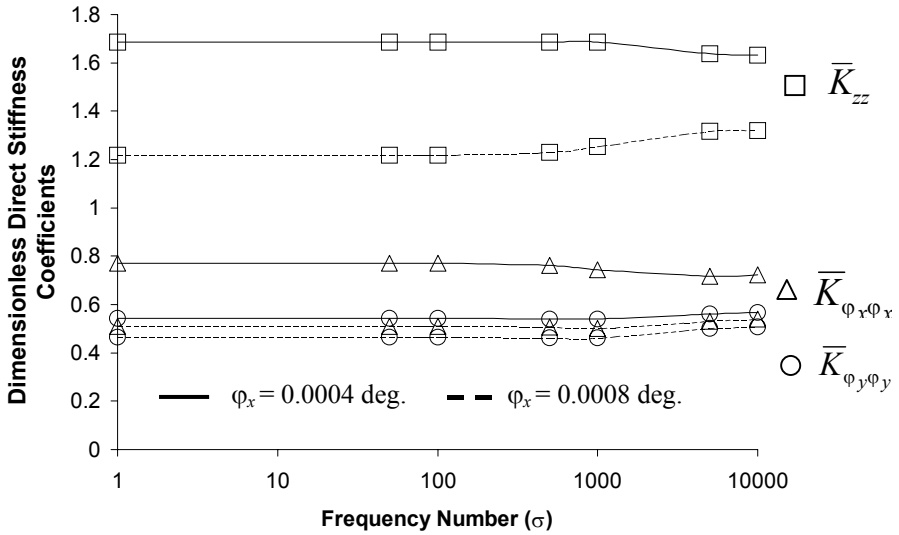

Figure 10. Dimensionless direct stiffness coefficients versus frequency number in a misaligned SGGFS (Λ=1253).

The gas seal analyzed is assumed to be perfectly balanced. The effects of the seal elastic support mechanism and damping associated with the secondary seal are not taken into account in the analysis. The seal elastic support mechanism is designed to act as a self-aligning element working against any change in the seal angular position.

6. Conclusions

This work presents a finite element study of misaligned spiral groove gas face seals operating at high speeds. Angular misalignment between seal faces is a common feature in gas seals operating under stringent conditions. A finite element procedure based on a high-order Galerkin weighted residual scheme is implemented to analyze some static and dynamic performance characteristics of spirally grooved gas seals. Curves of seal opening force, flow rate, direct and cross-coupled stiffness coefficients are obtained in relation to the static misalignment angle of the seal face. The finite element predictions indicate that seal misalignment results in increased seal opening force and stiffness coefficients offering increasing resistance to rubbing contact between the seal mating faces.

7. References

Bonneau, D., Huitric, J. and Tournerie, B., 1993, "Finite Element Analysis of Grooved Gas Thrust Bearings and Grooved Gas Face Seals", ASME Journal of Tribology, Vol.115, pp. 348-354.

Burgmann Dichtungswerke GmbH & Co., 1997, "Gas Lubricated Mechanical Face Seals", 1st Edition, Wolfratshausen, Germany. 76 p.

Etsion, I., 1979, "Hydrodynamic Effects in a Misaligned Radial Face Seal", ASME Journal of Lubrication Technology, Vol. 101, pp. 283-292.

Faria, M.T.C., 2001, "An Efficient Finite Element Procedure for Analysis of High-Speed Spiral Groove Gas Face Seals", ASME Journal of Tribology, Vol.123, No. 1, pp.205-210.

Green, I., 1987, "The Rotor Dynamic Coefficients of Coned-Face Mechanical Seals with Inward and Outward Flow", ASME Journal of Tribology, Vol. 109, pp. 129-135

Hernandez, P. and Boudet, R., 1995, "Modelling of the Behaviour of Dynamical Gas Seals: Calculation with a Finite Element Method Implicitly Assuring the Continuity of Flow", Proc. Instn. Mech. Engrs., Part J: Journal of Engineering Tribology, Vol.209, pp. 195-201.

Jang, G.H., and Kim, Y.J., 1999, "Calculation of Dynamic Coefficients in a Hydrodynamic Bearing Considering Five Degrees of Freedom for a General Rotor-Bearing System", ASME Journal of Tribology, Vol.121, No. 3, pp. 499-505.

Klostermann, G.E., 1999, "High Pressure Noncontacting Mechanical Seal for API Applications", Proceedings of the 16th International Pumper Users Symposium, Houston, USA, pp. 17-24.

Lund, J.W., 1987, "Review of the Concept of Dynamic Force Coefficients for Fluid Film Journal Bearings", ASME Journal of Tribology, Vol.109, No. 1, pp. 37-40.

Muijderman, E.A., 1966, "Spiral Groove Bearings", Philips Technical Library, Springer-Verlag, New York, 212 p.

Pan, C.H.T. and Sternlicht, B., 1967, "Thermal Distortion of Spiral-Grooved Gas Lubricated Thrust Bearing Due to Self-Heating", ASME Journal of Lubrication Technology, Vol. 89, pp. 197-202.

Tournerie, B., Huitric, J., Bonneau, D. and Frene, J., 1994, "Optimisation and Performance Prediction of Grooved Face Seals for Gases and Liquids", Proceedings of the 14th International Conference on Fluid Sealing, Firenze, Italy, pp. 351-365.

Wu, S., Kowalski, C.A. and Stafford, L.E., 1999, "Development of a Twin Hybrid Noncontacting Gas Seal and Its Application to Process Pumps", Proceedings of the 16th International Pumper Users Symposium, Houston, USA, pp. 59-67.

Zirkelback, N.L. and San Andrés, L., 1999, "Effect of Frequency Excitation on the Force Coefficients of Spiral Groove Gas Seals", ASME Journal of Tribology, Vol.121, No. 4, pp. 853-863.